Interface Dynamic Shear Characteristics of Aging GMB/CCL Composite Liner

Dian Chen[1]; Yong-Gui Chen[2]; Yong-Feng Deng[3]; Wei-Min Ye[4]; Dai-Cheng Ye[5]; and Juan Hou[6]

Abstract: Aging degradation of the geomembrane (GMB) significantly influences the dynamic shear characteristics of the composite liner interface, which comprises the GMB and the compacted clay liner (CCL), potentially jeopardizing the dynamic stability of landfills. In this study, cyclic shear tests were performed on two types of aging GMB/CCL interfaces, concurrently with shear tests on the nonaging GMB/CCL interface for comparison. The results suggest that the impact of aging on the dynamic shear characteristics of the GMB/CCL interface is essentially governed by the surface roughness and brittleness of the GMB, with the effect degree of brittleness influenced by the normal stress. Under low normal stress, aging increased the vertical displacement, dynamic shear strength, and shear stiffness of the GMB/CCL interface. However, under high normal stress, the dynamic shear strength and shear stiffness of the aging GMB/CCL interface were more likely to be lower than those of the nonaging interface. As the displacement amplitude increased, the influence of aging on the shear stiffness of the GMB/CCL interface gradually diminished. Aging also reduced the damping ratio of the GMB/CCL interface. The difference in vertical displacement between the exposed GMB/CCL interface and the in soil GMB/CCL interface caused by brittleness was not significant. In practical engineering, when the overlying load on the GMB/CCL composite liner is relatively small, aging makes the GMB more susceptible to tearing under seismic loads, whereas with larger overlying loads, aging is more likely to increase the shear displacement, thereby increasing the likelihood of instability in landfill. Finally, based on classic models of soil, fitting models for the normalized shear stiffness and damping ratio of the GMB/CCL interface were established and validated. This study can provide reference for analyzing the dynamic stability of landfills during long-term use. **DOI: 10.1061/JGGEFK.GTENG-12563.**

Author keywords: Aging geomembrane; Compacted clay liner (CCL); Cyclic shear test; Dynamic shear characteristics.

Introduction

In the design and operation of landfills, impermeability technology plays a crucial role in preventing leachate leakage and ensuring groundwater safety (Rowe 2005). Geomembrane (GMB), due to its excellent impermeability, is increasingly used as impermeable materials in landfills and are often combined with compacted clay liner (CCL) or geosynthetic clay liners (GCL) to form composite liner systems (Dickinson and Brachman 2008; Sirieix et al. 2016). While composite liners effectively prevent leachate from contaminating the surrounding environment, the shear strength of the composite liner interface is relatively low. There is a risk of sliding instability and failure along this interface in landfills, as exemplified by the overall sliding that occurred along the GMB/CCL interface at the Kettleman Hills Landfill in California in 1988 (Mitchell et al. 1990). Therefore, studying shear characteristics of composite liner interfaces holds significant importance for the thoughtful design of contemporary landfills and ensuring their stability.

Commonly used experimental methods for studying shear behavior of interfaces include large-scale direct shear tests (Fox and Ross 2011; Hanson et al. 2015; Lin et al. 2018; Feng et al. 2022), torsional ring shear tests (Stark and Poeppel 1994; Qian et al. 2011; Liu et al. 2023), and inclined plane tests (Pitanga et al. 2009; Carbone et al. 2015; Pavanello et al. 2021). In recent years, dynamic shear characteristics of these interfaces in landfill have gradually become one of the focal points in the environmental geotechnical field (Chang and Feng 2022). Yegian and Lahlaf (1992) initially utilized a horizontal shear plane vibration table to assess the dynamic shear strength of the GMB/nonwoven geotextile (NW GTX) interface. Subsequent researchers conducted a series of related studies through vibration table tests (De and Zimmie 1998; Kim et al. 2005; Carbone et al. 2015; Pavanello et al. 2018). However, vibration table tests suffer from significant drawbacks, particularly the application of relatively low normal stress to specimens, which does not align with the high-stress conditions experienced by composite liners in practical engineering applications. Dynamic direct shear tests can apply high normal stresses to specimens in accordance with actual conditions; previous researchers

[1]Doctoral Candidate, Dept. of Geotechnical Engineering, College of Civil Engineering, Tongji Univ., Shanghai 200092, China. Email: dian@tongji.edu.cn

[2]Professor, Dept. of Geotechnical Engineering, College of Civil Engineering, Tongji Univ., Shanghai 200092, China (corresponding author). ORCID: https://orcid.org/0000-0002-6571-2549. Email: cyg@tongji.edu.cn

[3]Professor, Institute of Geotechnical Engineering, School of Transportation, Southeast Univ., Nanjing 211189, China. ORCID: https://orcid.org/0000-0002-8223-8711. Email: noden@seu.edu.cn

[4]Professor, Dept. of Geotechnical Engineering, College of Civil Engineering, Tongji Univ., Shanghai 200092, China. Email: ye_tju@tongji.edu.cn

[5]Engineer, Xiamen Baicheng Construction & Investment Co., Ltd., 281 Lianqian West Rd., Siming District, Xiamen, Fujian 361009, China. Email: 13950070099@163.com

[6]Professor, School of Mechanics and Engineering Science, Shanghai Univ., Shanghai 200444, China. Email: juanhou@staff.shu.edu.cn

Note. This manuscript was submitted on December 12, 2023; approved on June 6, 2024; published online on August 29, 2024. Discussion period open until January 29, 2025; separate discussions must be submitted for individual papers. This paper is part of the ***Journal of Geotechnical and Geoenvironmental Engineering***, © ASCE, ISSN 1090-0241.

have employed this method for conducting some studies. Fox et al. (2011) conducted experimental research on the dynamic shear characteristics of interfaces between various GMB materials and compacted gravelly sand using a large-scale dynamic direct shear apparatus, revealing that, compared with high-density polyethylene (HDPE) GMB, linear low-density polyethylene (LLDPE) GMB exhibited higher shear stress but lower shear stiffness and damping at the interface with compacted gravelly sand. Chang et al. (2021) observed that the hysteresis loop of the GMB/GCL composite liner interface approximated a parallelogram; the loading frequency had little effect on the maximum shear stress and softening process; further, with an increase in load cycles, the secant shear stiffness decreased while the damping ratio increased. Chang and Feng (2021) found that displacement amplitude, normal stress, hydration conditions, and displacement rate are the primary influencing factors of the dynamic shear characteristics at the textured GMB/NW GTX interface. Besides the aforementioned geotechnical interfaces, GMB/CCL composite liners represent another important combination of geosynthetic materials that have been widely utilized in landfills for decades (Fox et al. 2014). However, research on the dynamic shear characteristics of GMB/CCL composite liner interfaces is currently limited (Feng et al. 2021).

Furthermore, HDPE GMB is composed of polymer resin (> 95%), carbon black (2%–3%), and antioxidants (0.5%–1%) (Hsuan and Koerner 1998). Over the extended period of use, GMB experiences aging degradation. The aging types of HDPE GMB are primarily classified as oxidative degradation (Rowe and Rimal 2008; Rowe and Shoaib 2018), radiation degradation (Tian et al. 2017), and thermal degradation (Rowe et al. 2010a). Oxidative degradation is the predominant form of degradation for HDPE GMB at the bottom of landfills (Rowe et al. 2010b). Oxidative degradation of GMB can be primarily categorized into three stages (Hsuan and Koerner 1998; Ewais et al. 2018): (1) depletion of antioxidants (stabilizers); (2) induction period of oxidative degradation; and (3) oxidative degradation period. During the construction of landfill liner, GMB may be exposed to sunlight for a certain period, leading to photooxidation degradation (Take et al. 2015).

Photooxidative degradation essentially involves the breaking of double bonds in the polymer molecular structure into free radicals under the influence of ultraviolet radiation. These free radicals rapidly combine with oxygen to form hydroperoxides, accelerating the degradation and cross-linking reactions of the polymer's high molecular chains (Suits and Hsuan 2003). Elevated temperatures can expedite both oxidative and photooxidative degradation processes (Kyrikou et al. 2011; Li et al. 2021). Scholars have conducted research on the physical and mechanical properties of aging GMB. Rowe et al. (2003) revealed that GMB exposed continuously to sunlight and high temperatures experienced greater degradation compared with GMB covered by leachate or soil, and were more prone to cracking under tensile stress. Rowe et al. (2010a) noted that the thicker the GMB, the slower its physical performance degraded, leading to a longer service life. Xue et al. (2013) observed that the tensile strength and puncture resistance of GMB decreased with increasing aging time and temperature. Arnepalli and Rejoice (2013) identified that exposure of GMB to ultraviolet radiation caused photooxidation, resulting in discoloration, surface cracking, brittleness, and long-term performance loss of GMB. Li et al. (2021) discovered that the sequence of factors affecting the antioxidant depletion period of GMB was aging method > brand/material > exposure medium > leachate composition > thickness. Anjana et al. (2023) found that exposure to ultraviolet radiation caused thickness to remain constant, density to decrease, yield stress to increase, yield strain to decrease, and tensile stress to decrease over extended degradation.

Currently, there are numerous old-age landfills in the world (Dos Santos et al. 2023), with liners composed of GMB and CCL. The aging degradation leads to a decline in the physical and mechanical properties of GMB, thereby affecting the dynamic shear characteristics of the GMB/CCL composite liner interface, posing a threat to the dynamic stability of landfills. However, research on the dynamic shear behaviors of aging GMB/CCL interfaces remains unexplored, underscoring the urgent need for relevant investigations.

In this study, employing a large-scale direct shear apparatus, cyclic loading with a sinusoidal waveform was applied to interfaces between three types of GMB (aging within the soil, aging externally exposed, and nonaging) and CCL, thus investigating the impact of aging on the vertical displacement, stress-displacement relationship, dynamic shear strength, dynamic shear stiffness, and damping ratio of the GMB/CCL interface. Ultimately, fitting models for the normalized shear stiffness and damping ratio of the GMB/CCL interface were established and validated, laying the groundwork for forecasting the dynamic stability of landfills during long-term use.

Test Methods

Materials and Apparatus

GMB specimens in this research consist of smooth HDPE GMB with a thickness of 1.5 mm. Aging GMB samples were obtained from the liner layer of a landfill in Xiamen City and were subjected to two different environmental conditions over approximately 18 years: burial within the soil; and exposure to the air. The original physical parameters of aging GMB were obtained from construction records, as shown in Table 1. The GMB buried in the soil (IS GMB) primarily underwent oxidative degradation during the 18-year period. However, the degree of degradation was much lower compared with the actual liner layer at the bottom of a landfill, as the oxidation occurred under conditions without overburden loads, high temperature, and infiltrating leachate. The externally exposed geomembrane (EX GMB) experienced photooxidative and oxidative degradation processes.

As for the nonaging GMB (NEW GMB) used for comparative study, its physical and mechanical parameters are as presented in Table 1. The original physical and mechanical parameters of the aging GMB closely resemble those of the NEW GMB.

The CCL is made of red clay in Xiamen City, with a specific gravity of 2.76, plastic limit (ω_P) of 26.8%, liquid limit (ω_L) of

Table 1. Physical and mechanical properties of HDPE GMB

Type	Thickness (mm)	Density (g/cm^3)	Yield strength (N/mm)	Tensile strength (N/mm)	Yield elongation (%)	Elongation at break (%)	Tear strength (N)	Puncture strength (N)
Aging GMB	1.5	0.94	≥20	≥38	≥13	≥700	—	—
NEW GMB	1.5	0.939	22	40	12	700	187	480

Note: Parameters of aging GMB refer to the parameters at the time of their production in the respective year.

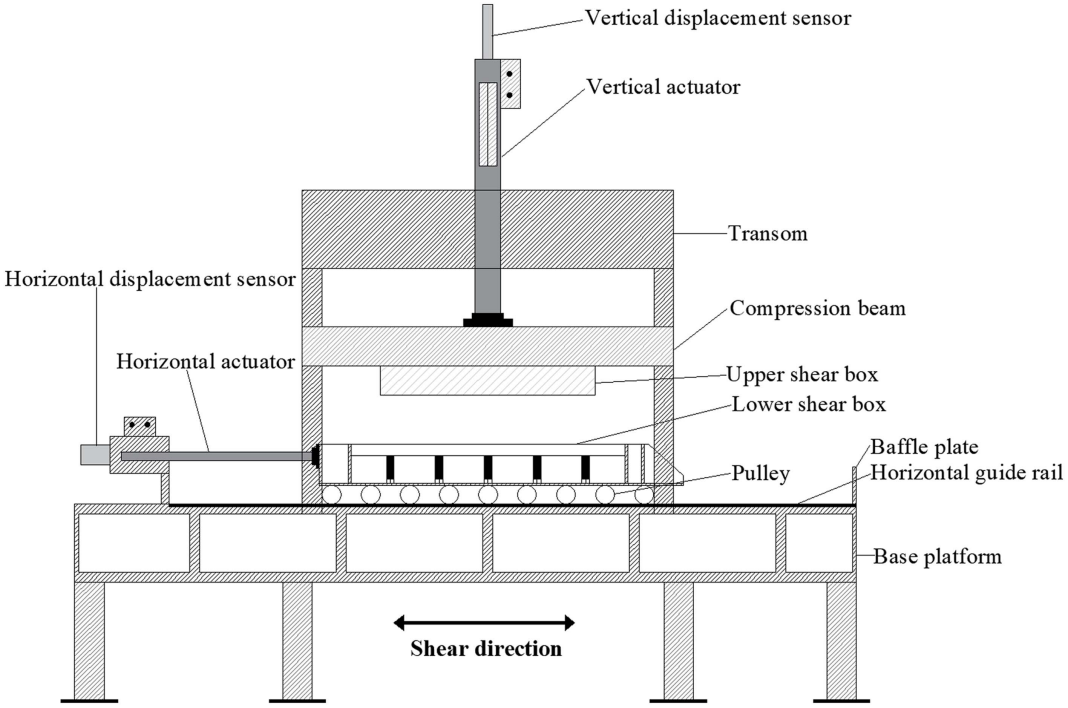

Fig. 1. Schematic diagram of the large direct shear apparatus.

51.9%, and plasticity index (I_p) of 25.1. According to ASTM D2487 (ASTM 2017a), it is classified as a high liquid limit clay. Compaction tests were conducted according to the requirements of ASTM D698 (ASTM 2021), and the maximum dry density ($\rho_{d\max}$) of the red clay was 1.76 g/cm^3.

The large direct shear apparatus is shown in Fig. 1. The apparatus primarily consists of a bidirectional actuator, bidirectional displacement sensors, and shear boxes. The dimensions of the upper shear box are 305 × 305 × 150 mm, while the lower shear box dimensions are 405 × 305 × 150 mm. The movement of the upper and lower boxes is controlled by an electrohydraulic servo system, with a maximum vertical output test force of 60 kN and a maximum horizontal output test force of 35 kN. The maximum shear displacement is 100 mm. Throughout the testing process, parameters such as normal stress, shear rate, and shear displacement are set and controlled by the computer's built-in software. Parameters, including shear stress, horizontal displacement, and vertical displacement, are automatically collected by the computer.

Test Procedures

Cyclic shear tests were conducted following ASTM D5321 (ASTM 2017b). Initially, a CCL specimen was prepared. The red clay was dried and pulverized. The compaction degree of the CCL specimen was set to 0.93 (Feng et al. 2021), requiring a minimum dry density of 1.64 g/cm^3. Multiplying this dry density by the volume of lower shear box yields the required dry weight of the CCL specimen. Controlling the moisture content of the clay is crucial, i.e., excessive moisture can make the CCL specimen too soft and prone to deformation, while insufficient moisture can result in a crack-prone specimen, affecting test results. After multiple attempts, the moisture content was determined to be 10%. Water was then added into the dry clay and mixed uniformly to achieve a moisture content of 10%. Subsequently, the mixture was placed in a sealed bag or container and left to stabilize for 24 h to ensure uniformity of the red clay. Using a layering method, the red clay was divided into three equal portions. Each layer of clay was compacted to a height of 50 mm using a compaction hammer. Before preparing the next layer, the surface of the CCL was scraped to prevent layering and ensure the uniformity of the CCL specimen. The final size of the CCL specimen was 405 × 305 × 150 mm (Fig. 2).

Cut the GMB into specimens of 300 × 300 mm, ensuring a constant shear area of 9 × 10^4 mm^2 during the shear process. Place the HDPE GMB specimen at the center of the CCL specimen. Attach 300 × 300 mm sandpaper to the upper shear box to prevent the GMB from moving with the CCL during shear. Gradually lower the upper shear box to ensure a precise fit between upper shear box and HDPE GMB on the CCL specimen. Apply the required normal stress (100, 200, and 400 kPa) through the vertical actuator

Fig. 2. CCL specimen.

Table 2. GMB/CCL composite liner cyclic shear test program

Test variables	Settings
Liner types	EX GMB/CCL, IS GMB/CCL, NEW GMB/CCL
Normal stress σ (kPa)	100, 200, 400
Displacement amplitude Δ (mm)	1, 5, 10
Frequency f (Hz)	0.1
Number of cycles N	60

for a period until there is no vertical displacement in the GMB/CCL interface. Then, initiate the horizontal actuator to apply cyclic shear loads.

This study performed a total of 27 displacement-controlled cyclic direct shear tests on three types of GMB/CCL interfaces: EX GMB/CCL interface; IS GMB/CCL interface; and NEW GMB/CCL interface. These tests were conducted at three normal stress levels ($\sigma = 100$, 200, and 400 kPa) and three displacement amplitudes ($\Delta = 1$, 5, and 10 mm). The cyclic loading was in the form of a sinusoidal waveform. Since the influence of loading frequency on the interface shear behavior is essentially the effect on the shear rate (Chang et al. 2021), with the same loading frequency, higher displacement amplitudes result in higher shear rates. Therefore, this study only conducted shearing at a single frequency. After conducting multiple preliminary shear tests on the GMB/CCL interface, it was observed that the test process was more stable at 0.1 Hz, making it more conducive to the subsequent analysis of the test results [note that 0.1 Hz falls within the frequency range of earthquakes (Ide et al. 2007; Uenishi 2018)]. The experiment concluded after 60 cycles of loading. Detailed information for the 27 tests can be found in Table 2.

Interface Dynamic Shear Characteristics of Aging GMB/CCL Interface

Surface of the Specimen after Shearing

Images of CCL and GMB specimens after shearing are presented in Fig. 3. The surface of the GMB specimen showed noticeable scratches, and some clay from the CCL specimen adhered to the GMB surface. Comparing the surfaces of specimens in Figs. 3(a and b), there was no significant difference, indicating that the impact of aging on the GMB/CCL interface requires detailed analysis, as presented in subsequent sections. Comparing Figs. 3(a and c), it is evident that, as the displacement amplitude increased, the damage to the IS GMB/CCL interface became more pronounced. Comparing Figs. 3(c and d), it can be observed that, with higher normal stress, the IS GMB specimen had fewer adhered clay particles on the surface, and the surface of CCL specimen appeared smoother. During the shear process, oscillating clay particles in the CCL specimen quickly bonded and compacted more efficiently at higher normal stresses, filling the voids in the CCL specimen.

Vertical Displacement Behaviors

If the composite liner system undergoes excessive vertical deformation, it may lead to cracking in the GMB. Therefore, studying the behavior of vertical displacement is crucial. The typical horizontal displacement–vertical displacement relationship curves for GMB/CCL interface are presented in Fig. 4. In the initial shear cycles, there was a rapid increase in vertical displacement, and the rate of change decreased in subsequent cycles. The fluctuation in the curves was attributed not only to specimen and instrumental factors but also to the excessively high sampling frequency ($f_s = 20$ Hz), which was much greater than the loading frequency ($f = 0.1$ Hz). Comparing Figs. 4(a–c), it was observed that, after 60 cycles, the vertical displacements (Y_-) corresponding to a displacement amplitude $\Delta = -10$ mm for EX GMB/CCL, IS GMB/CCL, and NEW GMB/CCL were 0.34, 0.36, and 0.45 mm, respectively. The vertical displacements (Y_+) corresponding to $\Delta = 10$ mm was 0.37, 0.38, and 0.5 mm, respectively, with differences of 0.03, 0.02, and 0.05 mm. The slope k of the vertical displacement line at the amplitude position for the 60th cycle is assumed to be

$$k = (Y_+ - Y_-)/2\Delta \tag{1}$$

According to Eq. (1), $k_{\text{EX GMB/CCL}} = 0.15\%$, $k_{\text{IS GMB/CCL}} = 0.1\%$, and $k_{\text{NEW GMB/CCL}} = 0.25\%$. The slope value was small, equivalent to a horizontal line, indicating that the vertical displacement hardly changed during the later stages of shear.

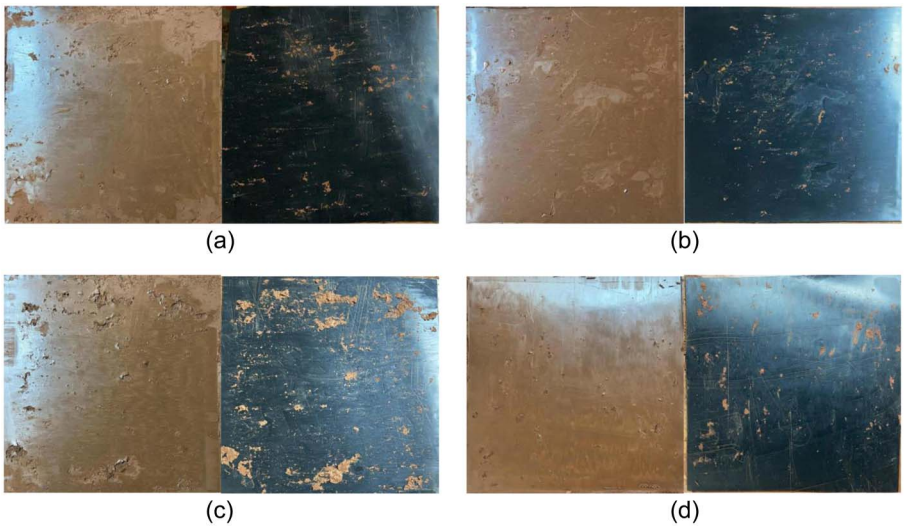

Fig. 3. CCL and GMB specimens after testing: (a) IS GMB/CCL-200 kPa-5 mm; (b) NEW GMB/CCL-200 kPa-5 mm; (c) IS GMB/CCL-200 kPa-10 mm; and (d) IS GMB/CCL-400 kPa-10 mm.

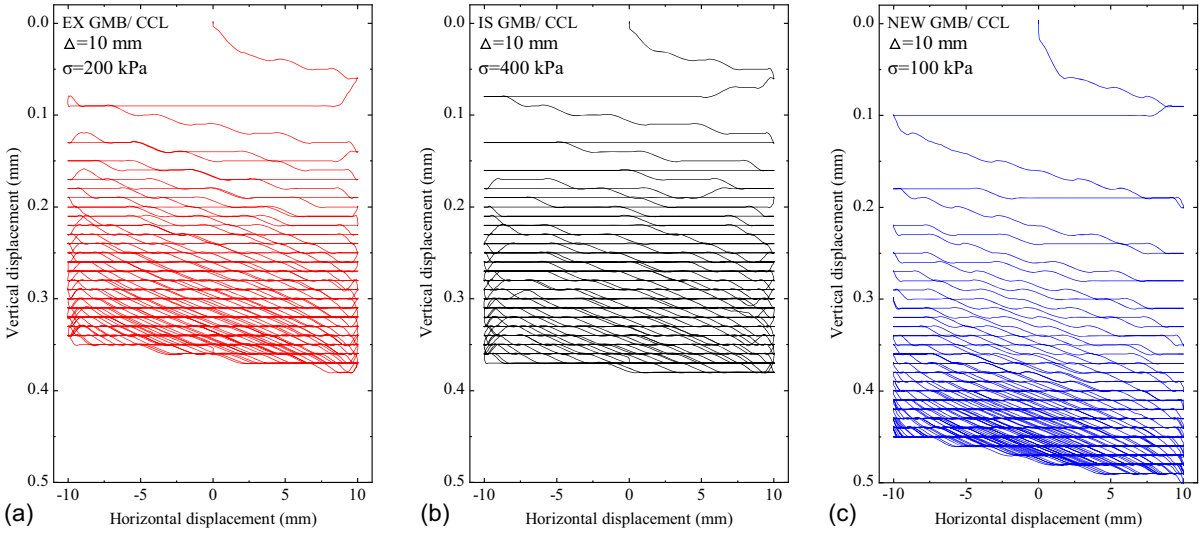

Fig. 4. Relationship between the vertical and horizontal displacement: (a) EX GMB/CCL-200 kPa-10 mm; (b) IS GMB/CCL-400 kPa-10 mm; and (c) NEW GMB/CCL-100 kPa-10 mm.

The vertical displacement behaviors under different normal stresses are depicted in Fig. 5. The vertical deformation of GMB/CCL composite liner increased rapidly with the number of cycles and gradually increased in subsequent cycles. Vertical deformation mainly occurred in the first 10 cycles. Taking 200 kPa normal stress as an example, for EX GMB/CCL composite liners at $\Delta = 1$, 5, and 10 mm, the vertical displacement in the first 10 cycles accounted for 79.5%, 72.2%, and 66.7% of the total displacement, respectively. For IS GMB/CCL composite liners, the corresponding values were 73.7%, 69.2%, and 69.0%; for NEW GMB/CCL composite liners, they were 70.0%, 70.0%, and 66.7%, respectively. This is mainly due to the significant sliding friction of CCL particles at the shear interface in the initial stage of cyclic shearing, where particle positions were adjusted, leading to a rapid increase in vertical displacement. Subsequently, the CCL particles became more compact, with increased interparticle interaction forces, requiring greater force for particle sliding, resulting in a gradual decrease in displacement increment.

The relationship between the total vertical displacement (i.e., final displacement) of each composite liner after 60 cycles of shear and the normal stress is shown in Fig. 6.

With increasing normal stress, the general trend for the total vertical displacement of NEW GMB/CCL composite liner was an increase. In contrast, no clear correlation between vertical displacement and normal stress was observed for EX GMB/CCL and IS GMB/CCL interfaces. This is attributed to the increased brittleness of EX GMB and IS GMB after degradation (Rowe et al. 2003; Abdelaal et al. 2014). Fig. 7 illustrates the cyclic shear process at the GMB/CCL interface. Under low normal stress ($\sigma = 100$ kPa), the interaction between GMB and CCL was minimal, and GMB can be considered planar during the shearing process. However, under high normal stress ($\sigma = 400$ kPa), the interaction between GMB and CCL increased, potentially causing GMB to bend during the shearing process. This also enlarged the contact area between GMB and CCL, leading to further rearrangement of CCL particles. Aging GMB was more brittle and less likely to deform without undergoing self-destruction. In contrast, the NEW GMB had greater deformation capacity, making it more susceptible to elastic deformation and subsequent bending during cyclic shear processes under high normal stress. Therefore, the vertical displacement of NEW GMB/CCL composite liner was more significantly correlated with normal stress.

There was no apparent pattern in the effect of displacement amplitude on the total vertical displacement of the GMB/CCL interface, as depicted in Fig. 6. Additionally, it can be also observed from Fig. 6 that, at $\sigma = 100$ and 200 kPa, the total displacement of the EX GMB/CCL interface exceeded that of the IS GMB/CCL and NEW GMB/CCL interfaces. This is attributed to prolonged exposure of the EX GMB to sunlight, leading to polymer degradation under ultraviolet radiation (Suits and Hsuan 2003), with its aging degree greater than that of IS GMB and NEW GMB, resulting in a rougher GMB surface. During cyclic shear processes, the EX GMB induced higher particle fragmentation and rearrangement in the CCL, resulting in a larger total displacement. However, as mentioned earlier, the total displacement of the NEW GMB/CCL interface was generally positively correlated with normal stress. At $\sigma = 400$ kPa, the total displacement of the NEW GMB/CCL interface exceeded that of the EX GMB/CCL and IS GMB/CCL interfaces. Further, the total displacement of the EX GMB/CCL interface was greater than that of the IS GMB/CCL interface at any normal stress and displacement amplitude. Since IS GMB and EX GMB have undergone 18 years of aging, the brittleness effect on total displacement was not significant, while the surface roughness of EX GMB is greater. When actual landfill engineering encounters earthquakes, aging increases the vertical deformation of GMB/CCL liners under smaller overburden loads, while the decreased mechanical properties of aging GMB make it more prone to tearing.

Stress-Displacement Relations

The stress-displacement curves are depicted in Figs. 8(a, c, and e). The dynamic response of the aging GMB/CCL and NEW GMB/CCL interfaces resemble that of the GMB/GCL interface (Chang et al. 2021), reaching peak shear strength rapidly in the initial stages of tests. The hysteresis loops for each interface shared a similar shape, forming an approximate parallelogram that gradually contracted with increasing cycle numbers, indicating stress degradation at the interface. However, after several cycles, the size of the hysteresis loop varied slightly, suggesting that interface

polishing and damage primarily occurred in the initial cycles of shear.

The stress-displacement curve in the initial stages of GMB/CCL interface is shown in Figs. 8(b, d, and f). It can be observed that the aging GMB/CCL interface and NEW GMB/CCL interface reached their maximum shear stress at very small displacements (around 1 mm) and then experienced a gradual stress reduction. After reaching the maximum horizontal displacement, the shear direction reversed, and the shear stress rapidly diminished to zero.

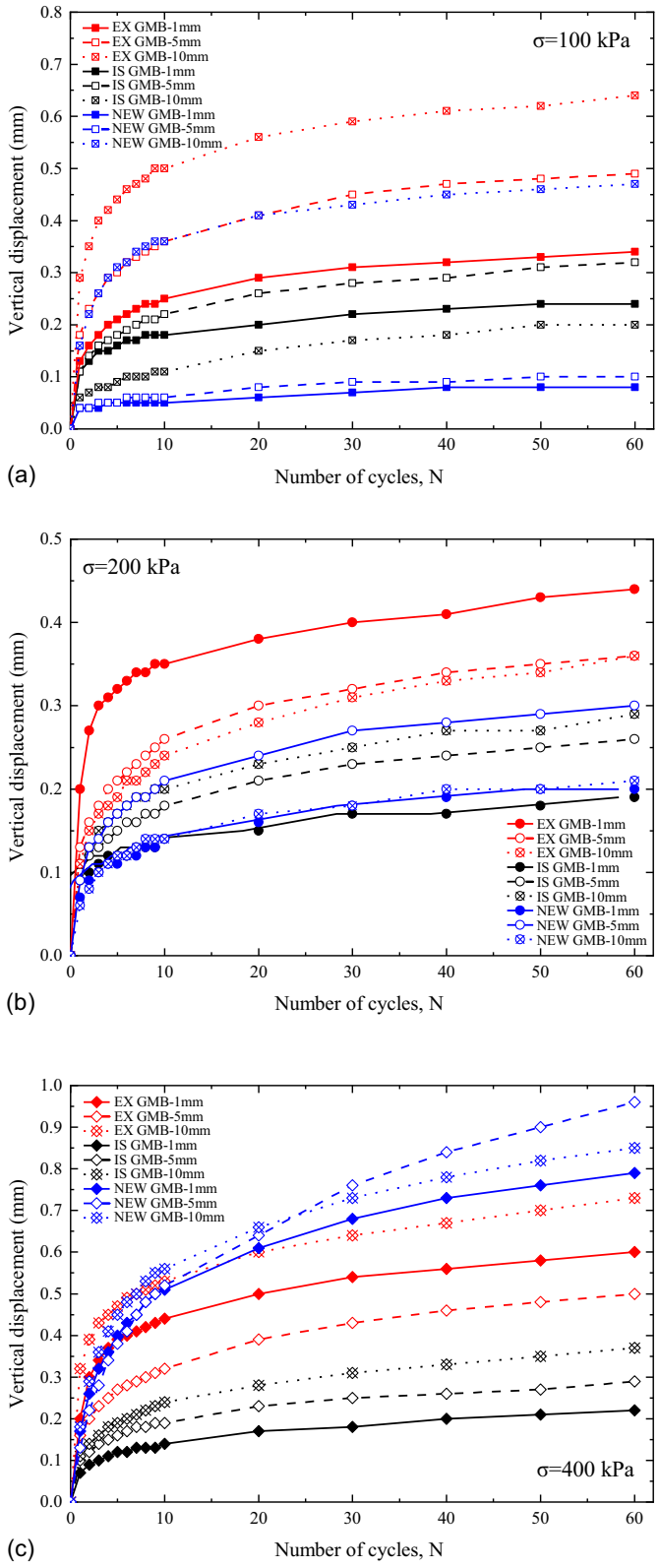

Fig. 5. Vertical deformation behavior under various normal stresses: (a) $\sigma = 100$ kPa; (b) $\sigma = 200$ kPa; and (c) $\sigma = 400$ kPa.

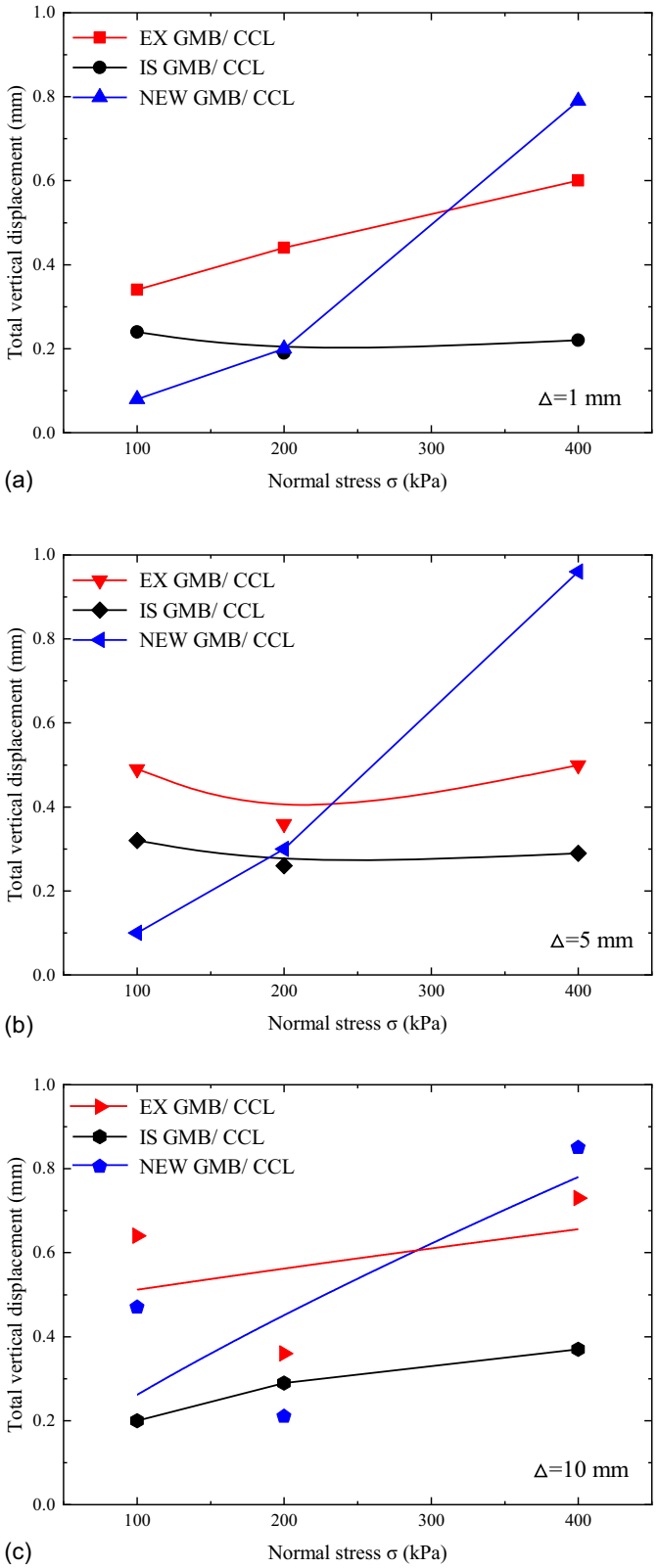

Fig. 6. Relationships between total vertical displacement and normal stress for various GMB/CCL interfaces under different displacement amplitudes: (a) $\Delta = 1$ mm; (b) $\Delta = 5$ mm; and (c) $\Delta = 10$ mm.

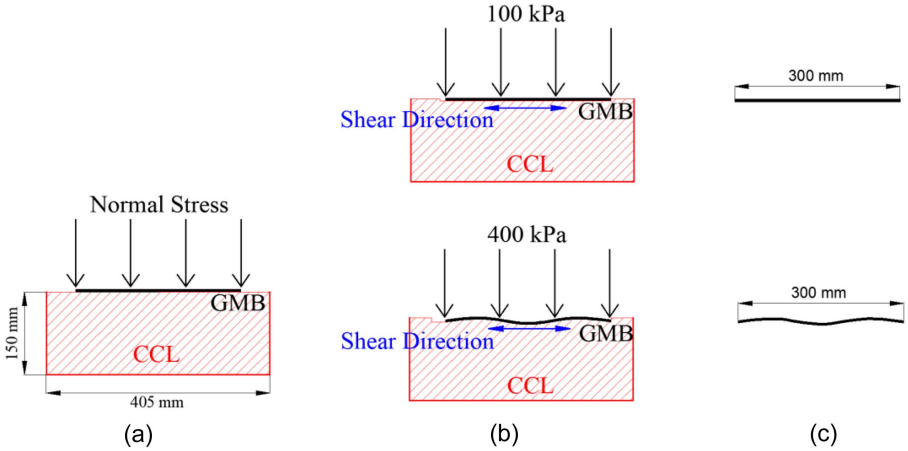

Fig. 7. Schematic diagram of the cyclic shear process for the GMB/CCL interface: (a) initial status; (b) shear process; and (c) GMB status.

In Feng et al. (2021), the GMB/CCL interface also exhibited stress softening, but the displacement at the peak shear stress in that study was much larger. This difference could be attributed to the use of high liquid limit clay in this study, which, unlike silty clay, had finer particles leading to a more rapid interface polishing and damage. From Figs. 8(b, d, and f), it is evident that the aging GMB/CCL and NEW GMB/CCL interfaces exhibited a decrease in initial shear stiffness with an increase in displacement amplitude, consistent with the behavior observed in other geotechnical interfaces (Chang et al. 2021; Chang and Feng 2021). Since the shear frequency in this study was constant at 0.1 Hz, and higher displacement amplitudes correspond to higher shear rates. Therefore, when a landfill experiences strong seismic events, the initial shear stiffness of GMB/CCL interface decreases, reducing its resistance to deformation, and the landfill may experience slip instability along this interface.

Dynamic Shear Strength

The maximum and minimum shear stresses of the geosynthetic interface are not completely symmetrical during cyclic shear (Wang et al. 2021). To better reflect the dynamic shear strength of the interface, the average maximum shear stress was chosen as the indicator of dynamic shear strength (Liu et al. 2021). The average maximum shear stress (τ_a) in a hysteresis loop is defined as the average of the absolute values of the maximum and minimum shear stresses within that hysteresis loop (Vieira et al. 2013). The interface peak strength (τ_p) is the maximum τ_a observed among all hysteresis loops, while the residual shear strength (τ_r) is the τ_a observed in the last hysteresis loop. Fig. 9 presents the relationship between the average peak shear strength (τ_a) and the number of cycles. τ_p for the aging GMB/CCL interface occurred in the first cycle, with three exceptions noted in the case of the NEW GMB/CCL interface. In Feng et al. (2021), a similar phenomenon was observed. Feng et al. (2021) attributed this to material variability. Notably, the EX GMB/CCL and IS GMB/CCL interfaces did not exhibit this variability.

In Fig. 9, the decay of τ_a mainly occurred in the first five cycles. For instance, at $\sigma = 400$ kPa, the reduction in τ_a over the first five cycles for the EX GMB/CCL interface at $\Delta = 1$, 5, and 10 mm accounted for 77.9%, 100%, and 91.4% of their respective maximum reductions. For the IS GMB/CCL interface, these values were 99.9%, 94.8%, and 88.6%; for the NEW GMB/CCL interface, they were 43.5%, 62.8%, and 69.0%. The relatively small percentage of 43.5% was attributed to the material variability discussed earlier. In the later stages of cyclic shearing, τ_a for the EX GMB/CCL and IS GMB/CCL interfaces might exhibit an increase at low normal stresses and low displacement amplitudes, indicating shear hardening. However, for the NEW GMB/CCL interface, this phenomenon occurred only at high normal stresses and high displacement amplitudes. Aging leads to a decrease in the mechanical properties of the EX GMB and IS GMB, rendering them more susceptible to wear in the later stages of cyclic shear. The surface roughness of the GMB increased, thus resulting in the observed shear hardening behavior at relatively low normal stresses and displacement amplitudes.

To more intuitively determine the relationship between peak shear strength (τ_p) and normal stress, linear fits were performed on the peak shear strength at various displacement amplitudes, as shown in Fig. 10. Overall, the peak shear strength of the GMB/CCL interface increased with the rise of normal stress. This is because, under high normal stress, the interaction forces between GMB and CCL increased, leading to an increase in the frictional forces between the clay particles at the contact surface. As a result, the shear stress required for particle rearrangement also increased. There was no significant relationship between peak shear strength and displacement amplitude.

Based on Fig. 10, it is observed that, at $\sigma = 100$ kPa, the peak shear strength of the EX GMB/CCL interface was the highest, followed by the IS GMB/CCL interface, with the NEW GMB/CCL interface exhibiting the lowest peak shear strength. This is attributed to the rougher surface of the EX GMB resulting from aging degradation. However, this trend changed when the normal stress increased to 200 kPa. At $\sigma = 200$ kPa and $\Delta = 5$ mm, the peak shear strength of the NEW GMB/CCL interface became the highest, while that of the EX GMB/CCL interface became the lowest, contrary to the previous trend. This is because the NEW GMB had the least brittleness, causing it to deform more elastically under increasing normal stress, thereby increasing the contact area with CCL particles and enhancing the shear resistance. However, at $\Delta = 1$ and 10 mm, the EX GMB/CCL interface still exhibited the highest shear stress compared with the IS GMB/CCL and NEW GMB/CCL interfaces, indicating that surface roughness still predominated. When the normal stress increased to 400 kPa, the peak shear strength of the NEW GMB/CCL interface was generally greater than that of the EX GMB/CCL interface, further demonstrating the significant influence of high normal stress on the GMB/CCL interface. However, when $\sigma = 400$ kPa and $\Delta = 1$ mm,

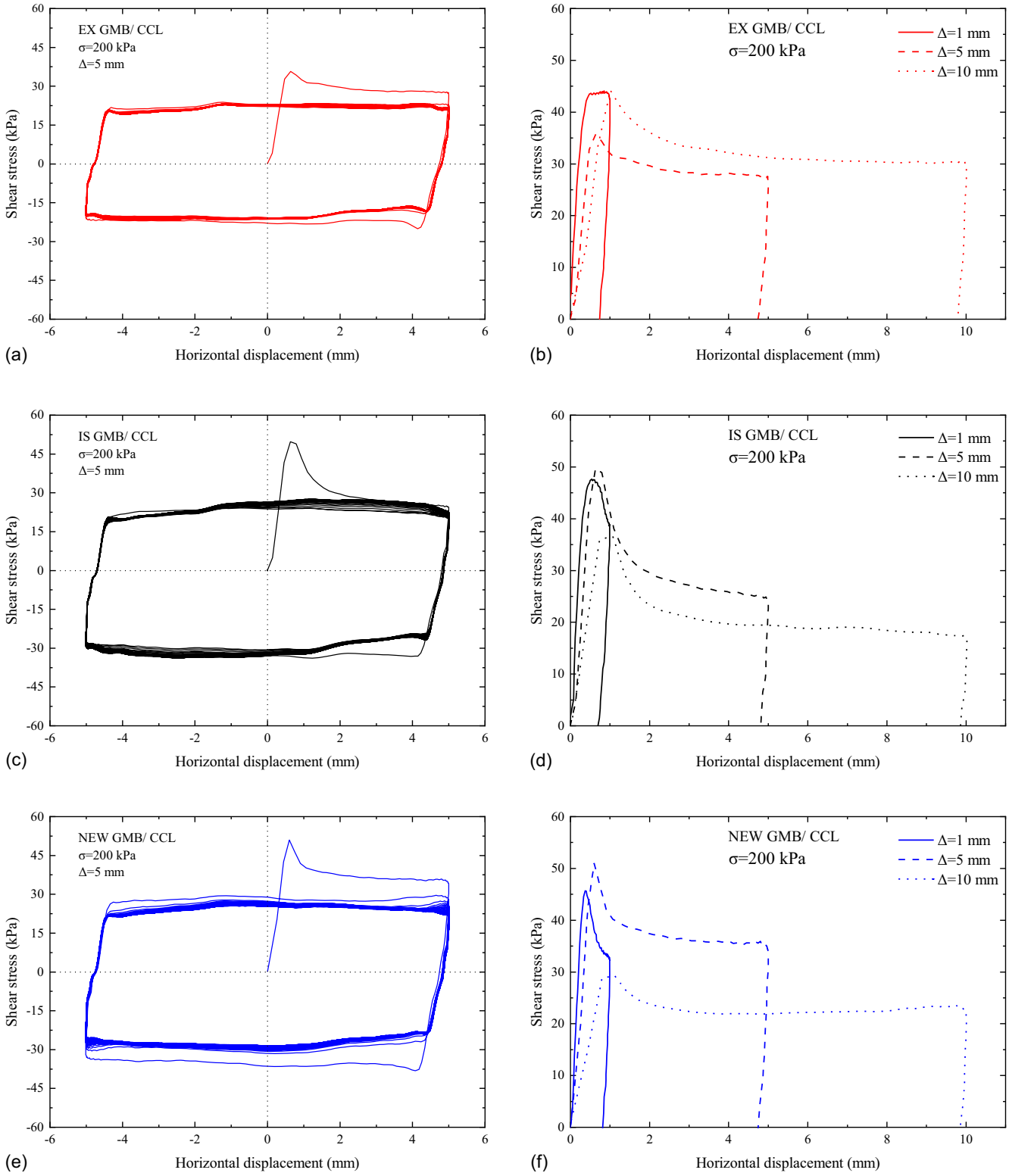

Fig. 8. (a, c, and e) Stress-displacement curve; and (b, d, and f) stress-displacement curve at the initial stage.

the IS GMB/CCL interface exhibited the highest peak shear strength. This is because the surface roughness and brittleness of the IS GMB were greater than that of the NEW GMB, with surface roughness predominating; while the surface roughness and brittleness of the IS GMB were less than that of the EX GMB, with brittleness predominating in this case.

In summary, the impact of aging on the peak shear strength of the GMB/CCL interface was primarily governed by the brittleness and roughness of the GMB surface, with the effect extent of brittleness influenced by the normal stress. Under low normal stress conditions, the peak shear strength of the aging GMB/CCL interface was greater than that of the NEW GMB/CCL interface. However, under high normal stress conditions, the peak shear strength of the NEW GMB/CCL interface was more likely to be greater than that of the aging GMB/CCL interface, although exceptions may occur. In such cases, surface roughness of the GMB predominated.

The relationship between residual shear strength (τ_r) and normal stress is depicted in Fig. 11. It can be observed that the residual shear strength of GMB/CCL interface generally increased with the rise of normal stress, with the fitting results being particularly good for the NEW GMB/CCL interface ($R^2 > 0.9$ for each line). Describing this linear relationship using the Mohr–Coulomb criterion, the relationship is expressed as

$$\tau_r = \sigma \tan \varphi_r + c_r \tag{2}$$

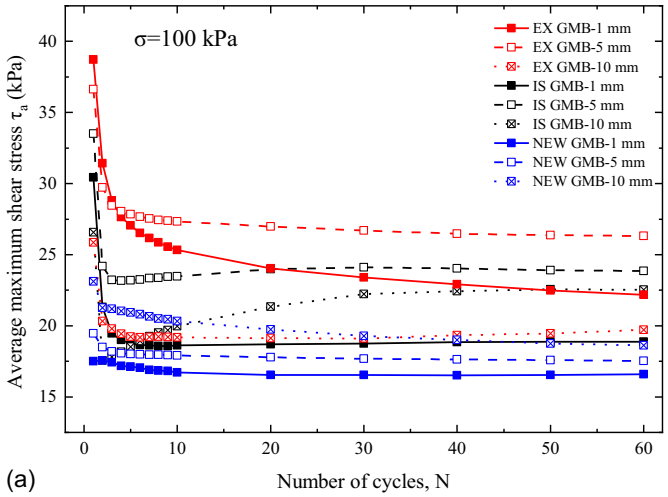

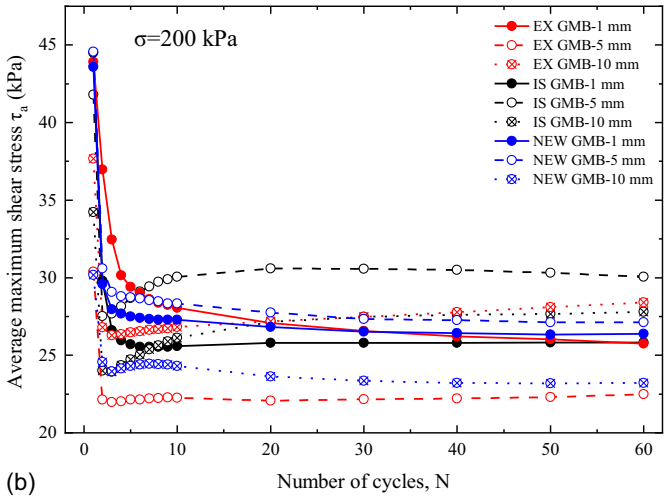

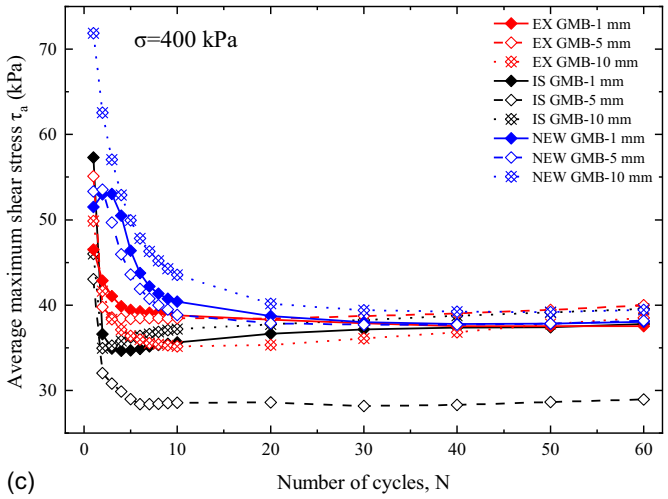

Fig. 9. Average maximum shear stress: (a) $\sigma = 100$ kPa; (b) $\sigma = 200$ kPa; and (c) $\sigma = 400$ kPa.

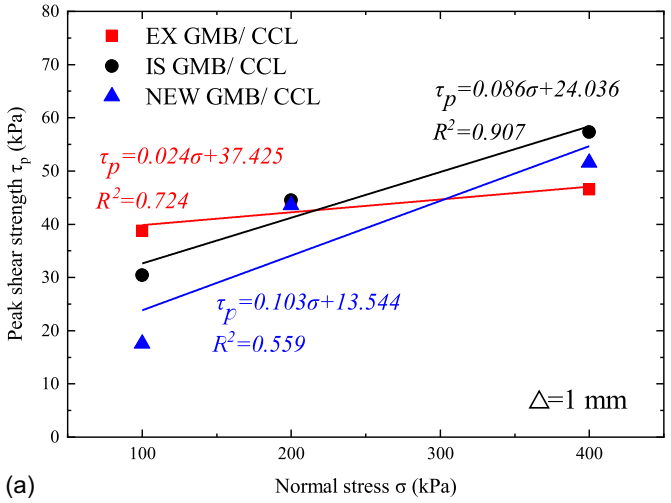

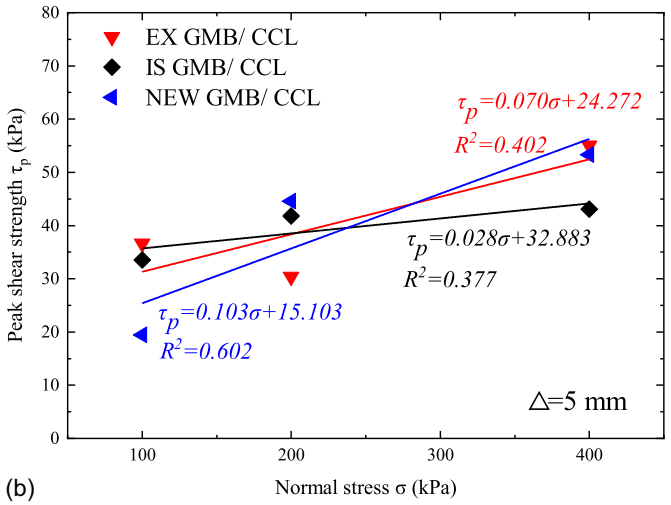

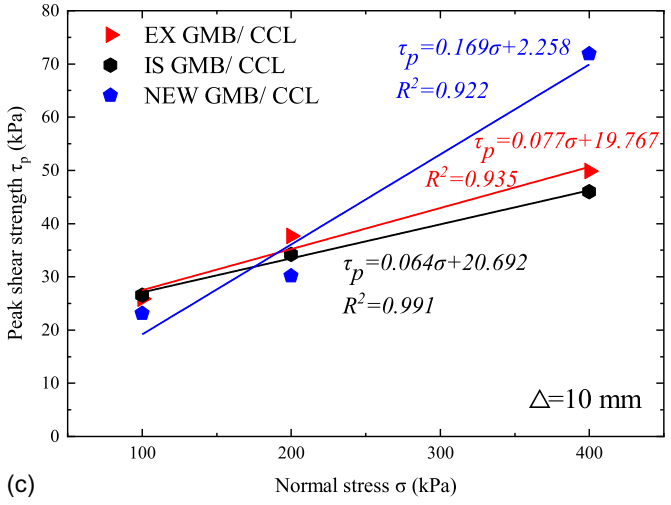

Fig. 10. Relationships between peak shear strength and normal stress for various GMB/CCL interfaces under different displacement amplitudes: (a) $\Delta = 1$ mm; (b) $\Delta = 5$ mm; and (c) $\Delta = 10$ mm.

where c_r and φ_r = the residual cohesion and residual internal friction angle of interface, respectively. The residual cohesion of NEW GMB/CCL interface corresponding to $\Delta = 1$, 5, and 10 mm was 10.764, 11.997, and 10.494 kPa, respectively, while the residual internal friction angles were 4.00°, 3.84°, and 4.06°, respectively. The displacement amplitude had minimal impact on the residual cohesion and residual internal friction angle of NEW GMB/CCL interface. In addition, there appeared to be no clear relationship between the residual shear strength and displacement amplitude for the GMB/CCL interfaces.

From Fig. 11, it is observed that, at $\sigma = 100$ and 200 kPa, the residual shear strength of the IS GMB/CCL interface was greater than that of the NEW GMB/CCL interface. In addition to being related to the initial roughness, it is also possible that the mechanical properties of the IS GMB decreased due to aging degradation, leading to its surface being more susceptible to wear and increased roughness after multiple cycles of shear, thereby gradually increasing the shear stress in the later stages of cyclic shear. However, the scenario reversed at $\sigma = 400$ kPa, where the dominance shifted to the brittleness of the GMB owing to increased normal stress. In the later stages of cyclic shear, the NEW GMB displayed greater elastic deformation, resulting in expanded contact area with particles on the polished CCL surface, thus enhancing shear resistance.

However, the phenomenon of greater residual shear strength at the EX GMB/CCL interface than the NEW GMB/CCL interface still occurred at $\sigma = 200$ and 400 kPa. The higher normal stress exacerbated the wear of the EX GMB after multiple cycles of shear. Although the increase in normal stress gradually enhanced the brittleness effect of the GMB, the dominance of surface wear was evident from the results. In summary, the influence of aging on the residual shear strength of the GMB/CCL interface was closely related to the normal stress. Under low normal stress, surface roughness predominated due to initial roughness and wear on GMB surfaces in the later stages of cyclic shear. With the increase in normal stress, the brittleness effect of the NEW GMB gradually intensified. Simultaneously, the degree of surface wear on the aging GMB was intensified under high normal stress. Both factors contribute to the increase in residual shear stress at the interface.

Dynamic Shear Stiffness and Damping Ratio

Shear stiffness and damping ratio are commonly used to characterize the dynamic response of specimens during cyclic shearing processes (Han et al. 2019; Liang et al. 2022), with detailed calculation methods described in relevant literature (Nye and Fox 2007; Wang et al. 2016).

Fig. 12 presents the relationship between the shear stiffness of various GMB/CCL interfaces and the normal stress or displacement amplitude at different numbers of cycles. According to Fig. 12, the shear stiffness of each GMB/CCL interface decreased with an increase in the number of cycles, except for the NEW GMB/CCL interface, which showed an increase in shear stiffness during the second cycle, attributed to the material variability mentioned earlier. In the later stages of cyclic shearing, slight increases in shear stiffness were observed for the EX GMB/CCL and IS GMB/CCL interfaces, attributed to the surface wear of the aging GMB, leading to increased surface roughness. As shown in Figs. 12(a, c, and e), at $\Delta = 1$ mm, the decrease in shear stiffness of the EX GMB/CCL interface mainly occured within the first five cycles; for the IS GMB/CCL interface, it occured within the first two cycles. However, for the NEW GMB/CCL interface, this number increased with the increase in normal stress. The surface of the EX GMB is rougher than that of the IS GMB and NEW GMB, thus requiring more cycles of shear to rearrange the CCL particles. The surface of the NEW GMB is smoother than that of the aging GMB, resulting in minimal interaction with CCL particles at $\sigma = 100$ kPa. Whereas under $\sigma = 400$ kPa, the lower brittleness of the NEW

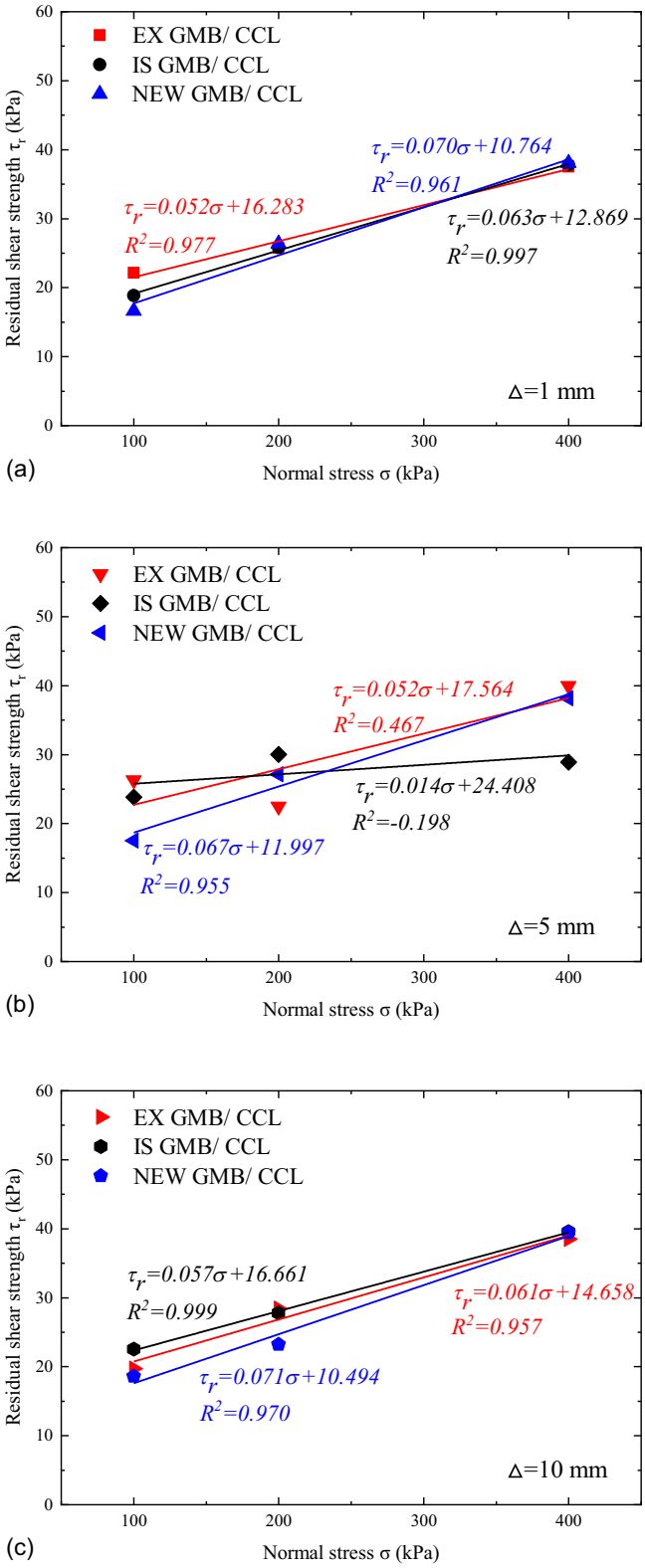

Fig. 11. Relationships between residual shear strength and normal stress for various GMB/CCL interfaces under different displacement amplitudes: (a) $\Delta = 1$ mm; (b) $\Delta = 5$ mm; and (c) $\Delta = 10$ mm.

GMB resulted in the decrease in shear stiffness primarily within the first 10 cycles. It is worth noting that, as depicted in Figs. 12(b, d, and f), when $\Delta = 5$ and 10 mm, the decrease in shear stiffness of each GMB/CCL interface occured within the first two cycles, indicating that the larger the displacement amplitude, the less the variation in shear stiffness of the GMB/CCL interface with the number of cycles.

From Figs. 12(a, c, and e), it can be observed that the shear stiffness of each GMB/CCL interface increased with the increase in normal stress for each cycle. In addition, it is evident from

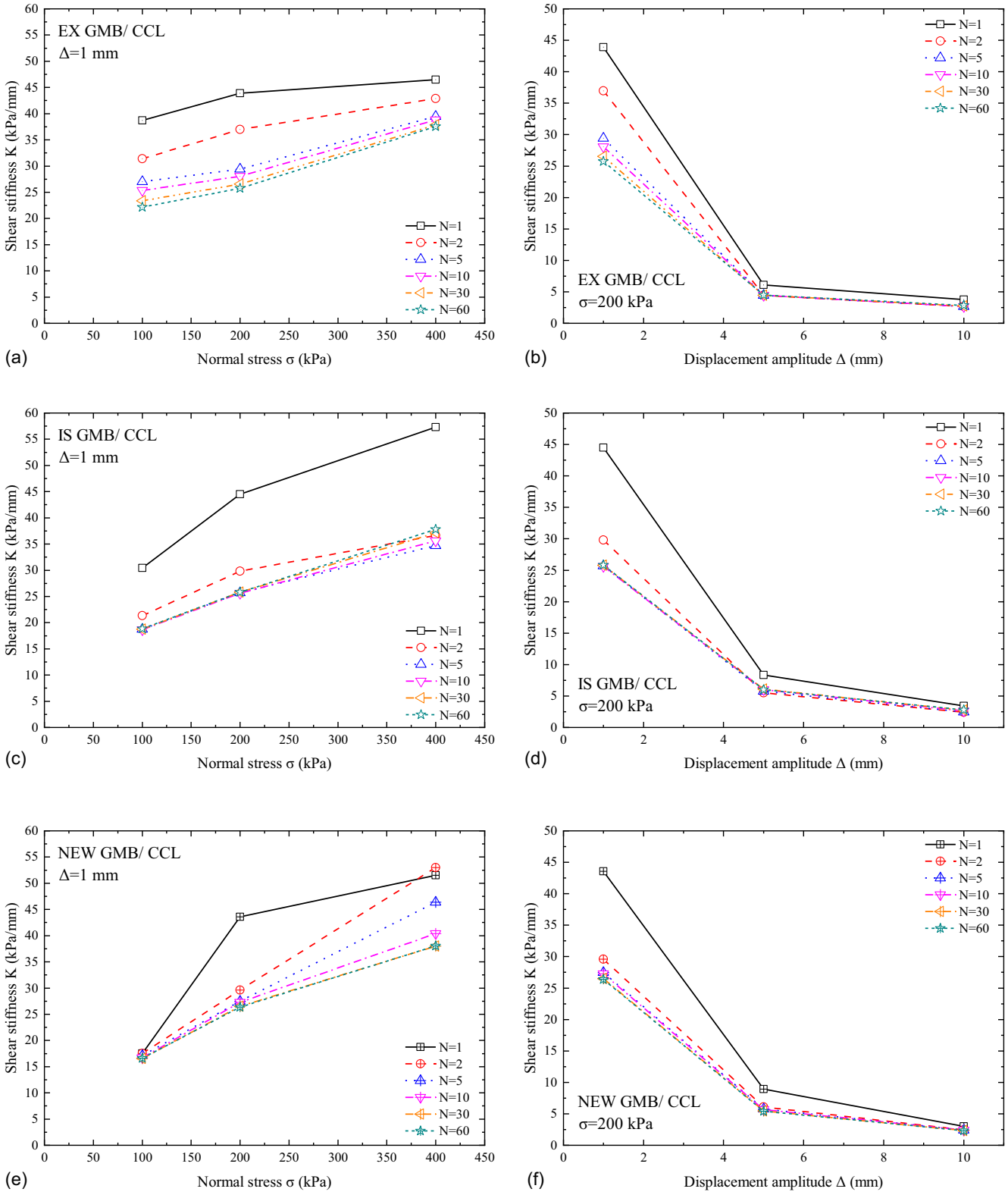

Fig. 12. (a, c, and e) Relationship between shear stiffness and normal stress; and (b, d, and f) relationship between shear stiffness and displacement amplitude.

Figs. 12(b, d, and f) that the shear stiffness of each GMB/CCL interface decreased with the increase in displacement amplitude for each cycle.

The maximum shear stiffness in all hysteresis loops is defined as the peak shear stiffness. Comparing Figs. 12(a, c, and e), when $\Delta = 1$ mm and $\sigma = 100$ kPa, the peak shear stiffness of the EX GMB/CCL interface was 21.2 kPa/mm higher than that of the NEW GMB/CCL interface, indicating that the roughness of the GMB surface dominated. When $\Delta = 1$ mm and $\sigma = 200$ kPa, the difference in peak shear stiffness between the two interfaces became very small (0.3 kPa/mm). At $\Delta = 1$ mm and $\sigma = 400$ kPa, the peak shear stiffness of the NEW GMB/CCL interface was 5.0 kPa/mm higher than that of the EX GMB/CCL interface, contrary to the previous relationship, as the increase in normal stress made the brittleness effect of GMB more pronounced. However, at $\Delta = 1$ mm and $\sigma = 400$ kPa, the peak shear stiffness of the IS GMB/CCL interface was 5.8 kPa/mm higher than that of the NEW GMB/CCL interface, indicating that, even under high normal stress, the initial roughness of the GMB surface still played a significant role in the interface peak shear stiffness. Comparing Figs. 12(b, d, and f), as the displacement amplitude increased, the difference in peak shear stiffness between each GMB/CCL interface decreased, and the influence of aging on the peak shear stiffness of the GMB/CCL interface decreased with the increase in displacement amplitude. The main reason may be that the increase in displacement amplitude caused greater disturbance to the CCL surface during shear, resulting in more severe damage, which had a much greater impact than aging.

Shear stiffness at 60th cycle is defined as the residual shear stiffness of the interface. Comparing Figs. 12(a, c, and e), it is observed that, at $\Delta = 1$ mm and $\sigma = 100$ kPa, the residual shear stiffness of the EX GMB/CCL interface was the highest, while that of the NEW GMB/CCL interface was the lowest. When $\Delta = 1$ mm and $\sigma = 200$ or 400 kPa, the residual shear stiffness of the NEW GMB/CCL interface exceeded that of the aging GMB/CCL interface. This is because, at low normal stress, the surface roughness of the aging GMB was higher, and it was more prone to wear in the later stages of cyclic shear, increasing the interaction force with the CCL, thus increasing the shear resistance and, consequently, the shear stiffness. Conversely, at high normal stress, the low brittleness effect of the NEW GMB gradually became more significant. However, as depicted in Figs. 12(b, d, and f), at $\sigma = 200$ kPa, the aging GMB/CCL interface at other displacement amplitudes still demonstrated a trend where the residual shear stiffness exceeded that of the NEW GMB/CCL interface. This indicates that, even under high normal stress, the surface roughness of the GMB still had a significant impact on the residual shear stiffness of the interface. According to Figs. 12(b, d, and f), it can be found that, similar to the peak shear stiffness, the influence of aging on the residual shear stiffness of the GMB/CCL interface gradually diminished with the increase in displacement amplitude.

The relationship curves between the damping ratio of each GMB/CCL interface and normal stress or displacement amplitude at different cycle numbers are presented in Fig. 13. As observed from Fig. 13, the damping ratio for the NEW GMB/CCL interface consistently increased with an increasing number of cycles, indicating a worsening degree of interface damage and a stronger ability to dissipate energy. For the EX GMB/CCL interface, the damping ratio increased with the number of cycles at low displacement amplitudes ($\Delta = 1$ mm); however, in the later stages of cyclic shearing with $\Delta = 5$ and 10 mm, the damping ratio slightly decreased with an increasing number of cycles. The pattern of damping ratio variation for the IS GMB/CCL interface was consistent with that of EX GMB/CCL interface, indicating that aging leads to a decrease in the damping ratio of GMB/CCL interface in the later stages of cyclic shearing. This is related to aging, which made GMB more prone to wear in the later stages of cyclic shear at the interface, leading to shear hardening.

From Figs. 13(a, c, and e), it is evident that the relationship between the damping ratio and normal stress for each GMB/CCL interface was not clear. Even at various cycle numbers, there were different variations in the trend of interface damping ratio with normal stress. According to Figs. 13(b, d, and f), the damping ratio generally increased with an increase in displacement amplitude, indicating that larger displacement amplitudes enhanced energy dissipation in the GMB/CCL interface. However, there was an exception: in the later stages of cyclic shearing, the damping ratio for $\Delta = 10$ mm was lower than that for $\Delta = 5$ mm in the IS GMB/CCL interface. This was attributed to the occurrence of shear hardening in the later stages of IS GMB/CCL interface. Comparing the damping ratios of each GMB/CCL interface at each cycle in Fig. 13, it is found that the damping ratio of the NEW GMB/CCL interface was generally greater than that of the aging GMB/CCL interface. Therefore, aging reduced the damping ratio of the GMB/CCL interface.

Discussions

Methods for dynamic analysis in landfill engineering mainly include the pseudostatic method (Qian and Koerner 2010), equivalent linear analysis method (Choudhury and Savoikar 2009), and nonlinear analysis method (Feng et al. 2018). The pseudostatic analysis method cannot consider the stress–strain relationship of materials, while the nonlinear analysis method, which employs constitutive models, involves complex model parameters and is not easily applicable. The equivalent linear method utilizes the equivalent linear model of materials, reflecting the relationship between shear modulus attenuation and damping ratio variation with strain under dynamic loads. It is easy to obtain model parameters, overcoming the shortcomings of the aforementioned methods; it's also one of the most commonly used methods for dynamic analysis in landfill. The accuracy of equivalent linear seismic analyses in landfills largely depends on the shear stiffness and damping ratio models of materials. However, equivalent-linear dynamic analysis in landfills often neglects the influence of the bottom liner, which is inconsistent with the actual situation and can lead to significant errors (Feng and Yang 2012). Additionally, there is currently no specific model to describe the shear stiffness and damping ratio of liner interfaces.

Since the variation trend of shear stiffness with displacement amplitude in this study was similar to the trend of shear modulus with shear strain in soils (Brennan et al. 2005; Sarkar and Sadrekarimi 2022), a similar method to soil shear modulus treatment was adopted here to normalize the shear stiffness at each displacement amplitude using the shear stiffness at $\Delta = 1$ mm of the interface. The results are shown in Fig. 14(a). It can be found that the shape of the curve of the relationship between the normalized shear modulus and the displacement amplitude of the GMB/CCL interface was similar to the classical Davidenkov model (Martin and Seed 1982) describing the $G/G_{\max}$-γ curve of soil. The expression of the Davidenkov model is as follows:

$$G/G_{\max} = 1 - H(\gamma) = 1 - \left[\frac{\left(\frac{\gamma}{\gamma_0}\right)^{2B}}{1 + \left(\frac{\gamma}{\gamma_0}\right)^{2B}}\right]^{A} \tag{3}$$

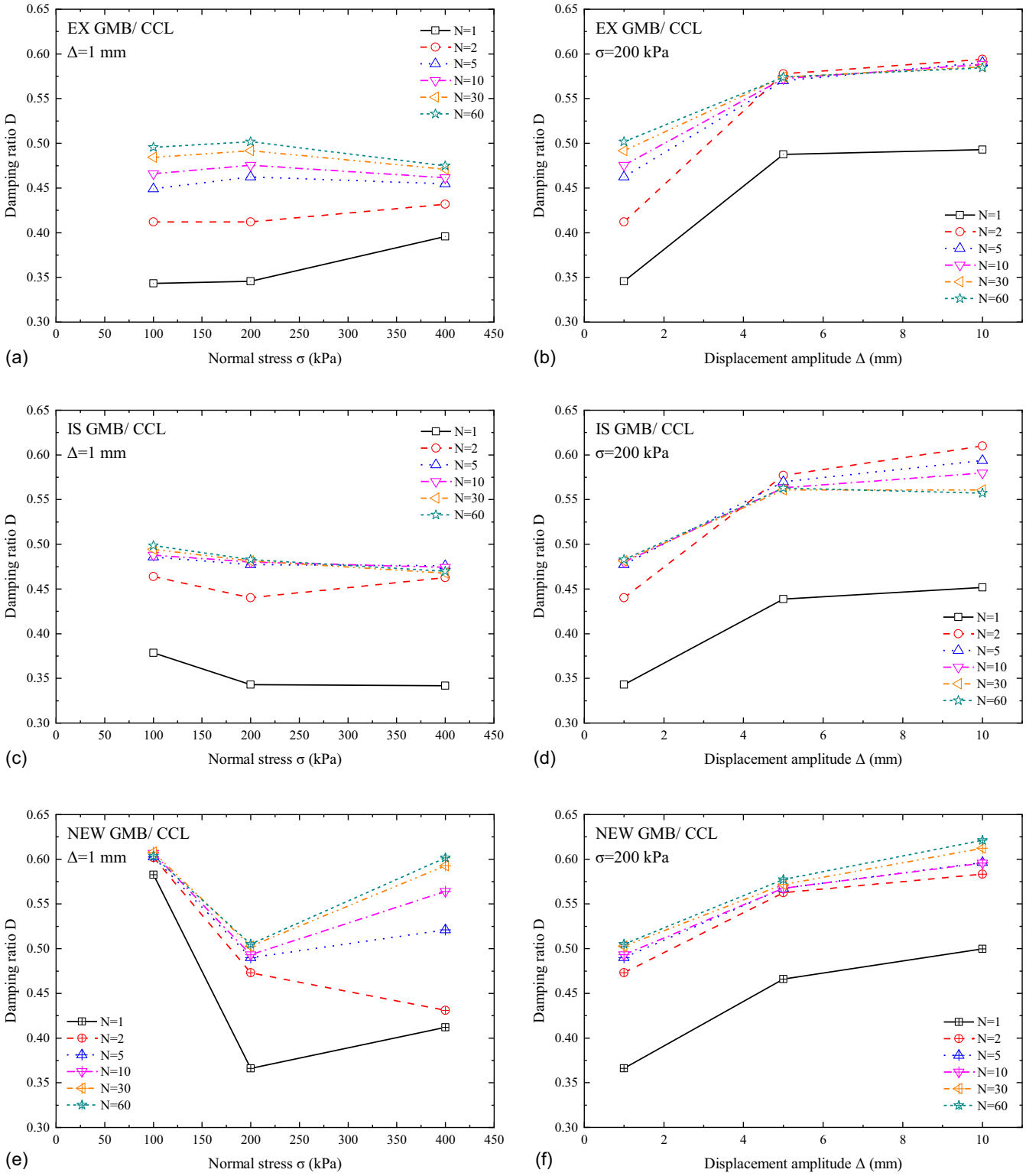

Fig. 13. (a, c, and e) Relationship between damping ratio and normal stress; and (b, d, and f) relationship between damping ratio and displacement amplitude.

where G = the shear modulus; G_{max} = the shear modulus at low strains; γ = the shear strain; and A, B, and γ_0 = the fitting parameters related to the properties of the soil. Since this study involves interface direct shear tests, the expression form of Eq. (3) was applied, using the displacement amplitude Δ instead of shear strain γ, and the shear stiffness K instead of shear modulus G, resulting in the following expression:

$$K/K_{max} = 1 - H(\Delta) = 1 - \left[\frac{(\frac{\Delta}{\Delta_0})^{2B}}{1 + (\frac{\Delta}{\Delta_0})^{2B}}\right]^{A} \quad (4)$$

where K_{max} = the shear stiffness at low displacement amplitudes (in this study, $\Delta = 1$ mm); and A, B, and Δ_0 are fitting parameters related to the GMB/CCL interface. Eq. (4) was utilized to fit

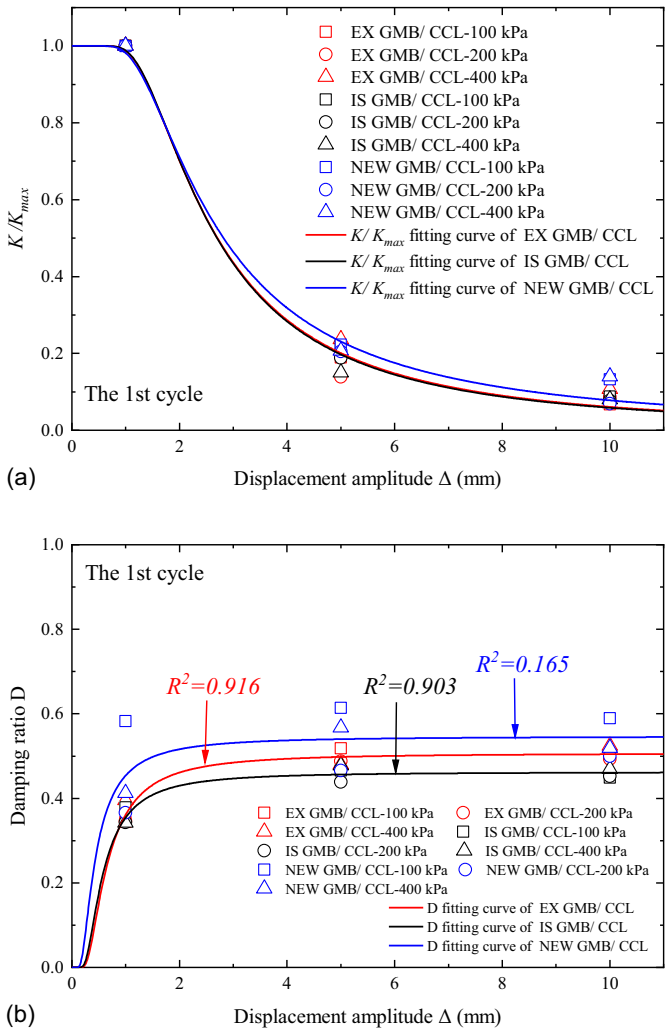

Fig. 14. Fitting curves on first cycle for: (a) normalized shear stiffness; and (b) damping ratio.

the experimental data of this study, verifying the applicability of Eq. (4) to the GMB/CCL interface.

The normalized shear stiffness fitting curves for EX GMB/CCL, IS GMB/CCL, and NEW GMB/CCL interfaces are shown in Fig. 14(a). The fitted parameters are presented in Table 3.

The R^2 values for the normalized shear stiffness fitting curves of EX GMB/CCL, IS GMB/CCL, and NEW GMB/CCL interfaces were all greater than 0.9, indicating a good fit. The Eq. (4) can effectively describe the relationship between shear stiffness and displacement amplitude for each GMB/CCL interface. The values of parameter A vary significantly, while the values of B and Δ_0 change relatively little, indicating that B and Δ_0 are critical parameters of Eq. (4).

For the damping ratio, Hardin and Drnevich (1972) used the following equation to describe the relationship between damping ratio and shear strain of soil:

$$D = D_{\max}(1 - G/G_{\max}) \tag{5}$$

where $D_{\max}$ = the maximum damping ratio. Building upon Eq. (5), Feng et al. (2021) employed the following formula to describe the relationship between the damping ratio of the GMB/CCL interface and the equivalent shear strain (γ_d):

Table 3. Model parameters

Parameters	EX GMB/CCL				IS GMB/CCL				NEW GMB/CCL			
	1st cycle	2nd cycle	5th cycle	60th cycle	1st cycle	2nd cycle	5th cycle	60th cycle	1st cycle	2nd cycle	5th cycle	60th cycle
A	1,767.535	1,771.02	1,764.677	1,717.247	1,818.726	1,805.62	1,741.456	1,660.311	1,624.703	1,659.076	1,643.864	1,696.177
B	0.91985	0.96646	0.92926	0.87219	0.93224	0.91277	0.87005	0.85059	0.84733	0.8626	0.86905	0.87384
Δ_0	0.03809	0.04485	0.03949	0.03177	0.03958	0.03692	0.0314	0.02916	0.02895	0.03075	0.03174	0.03213
R^2 $(K/K_{\max})$	0.99233	0.99404	0.99561	0.99453	0.9957	0.99637	0.99386	0.98986	0.99145	0.99432	0.99426	0.99594
D_0	0.5068	0.58408	0.58968	0.59065	0.46247	0.60855	0.61891	0.61013	0.54671	0.59347	0.60323	0.62405
B	0.07816	0.07585	0.05951	0.04431	0.06022	0.06592	0.05939	0.05546	0.04628	0.04088	0.02789	0.02172
R^2 (D)	0.91561	0.94156	0.94476	0.94018	0.90296	0.89197	0.60351	0.32894	0.16539	0.33892	0.3367	0.2494

$$D = D_0(1 - K/K_{\max})^{\beta} \quad (6)$$

where D_0 and β = the fitting parameters. Considering that the interfaces in this study are all GMB/CCL interfaces, the equivalent shear strain γ_d was replaced by displacement amplitude. Hence, Eq. (6) was transformed into the following expression:

$$D = D_0(H(\Delta))^{\beta} \quad (7)$$

The experimental data of this study were fitted using Eq. (7), and the fitting results are shown in Fig. 14(b). The fitted parameters are presented in Table 3. According to the R^2 values of the fitting curves, the damping ratio fitting results for the EX GMB/CCL interface were relatively good, indicating that Eq. (7) can well describe the relationship between damping ratio and displacement amplitude for the EX GMB/CCL interface. The damping ratio fitting results for the IS GMB/CCL interface were good only in the first two cycles, while the fitting results for the NEW GMB/CCL interface were not satisfactory in all cycles. Further, the influence of normal stress on the damping ratio of IS GMB/CCL and NEW GMB/CCL interfaces was more significant, resulting in more scattered experimental data and making it difficult to achieve a good fit.

Conclusions

Through the analysis of dynamic shear test results on aging GMB/CCL composite liners, the main conclusions obtained are as follows:

1. The vertical displacement of the NEW GMB/CCL interface generally increased with the increase in normal stress, whereas this trend was not observed in the aging GMB/CCL interface. Under 100 kPa normal stress, the vertical displacement of the aging GMB/CCL interface was greater than that of the NEW GMB/CCL interface; however, the opposite result was observed under 400 kPa normal stress. When the overlying load on the GMB/CCL composite liner is relatively small, aging increases the interface's vertical displacement under seismic loads, and, due to the decreased mechanical properties of the aging GMB, it is more prone to tearing.
2. The dynamic shear strength and shear stiffness of the GMB/CCL interface generally increased with increasing normal stress. Aging significantly influences the dynamic shear strength and shear stiffness of the GMB/CCL interface, with a strong correlation to normal stress. Under 100 kPa normal stress, aging increased the peak shear strength and shear stiffness of the GMB/CCL interface; however, under 400 kPa normal stress, the NEW GMB/CCL interface was more likely to be greater than the aging GMB/CCL interface. As the displacement amplitude increased, the influence of aging on the shear stiffness of the GMB/CCL interface decreased. Aging also reduced the damping ratio of the GMB/CCL interface. When the overlying load on the GMB/CCL composite liner is relatively large, aging increases the interface shear displacement under seismic loads, thereby increasing the likelihood of instability in landfill.
3. Aging caused the GMB/CCL interface to undergo shear hardening more readily in the later stages of cyclic shearing, resulting in a slight increase in dynamic shear strength and shear stiffness and a decrease in damping ratio.
4. The influence of aging on the dynamic shear characteristics of the GMB/CCL interface is essentially governed by the surface roughness and brittleness of the GMB, with the effect degree of brittleness affected by the normal stress.
5. Based on classic models of soil, fitting models for the normalized shear stiffness and damping ratio of the GMB/CCL interface were established. The fitting results for the normalized shear stiffness of each GMB/CCL interface were good, while the fitting model for the damping ratio was only applicable to the EX GMB/CCL interface.

Data Availability Statement

All data that support the findings of this study are available from the corresponding author upon reasonable request.

Acknowledgments

The work was supported by the National Natural Science Foundation of China (Grant Nos. 42125701 and 51978390), Innovation Program of Shanghai Municipal Education Commission (2023ZKZD26), Fund of the Shanghai Science and Technology Commission (22DZ2201200), Fujian Provincial Transportation Technology Project (202265), and the Top Discipline Plan of Shanghai Universities-Class I and Fundamental Research Funds for the Central Universities. The authors would like to extend their most sincere gratitude to the editors and reviewers who provided help with this paper.

References

Abdelaal, F. B., R. K. Rowe, and R. W. I. Brachman. 2014. "Brittle rupture of an aged HPDE geomembrane at local gravel indentations under simulated field conditions." *Geosynth. Int.* 21 (1): 1–23. https://doi.org/10.1680/gein.13.00031.

Anjana, R. K., S. Keerthana, and D. N. Arnepalli. 2023. "Coupled effect of UV ageing and temperature on the diffusive transport of aqueous, vapour and gaseous phase organic contaminants through HDPE geomembrane." *Geotext. Geomembr.* 51 (2): 316–329. https://doi.org/10.1016/j.geotexmem.2022.11.005.

Arnepalli, D. N., and A. A. Rejoice. 2013. "Service life and long-term performance of geosynthetic liners under simulated landfill conditions." In *Proc., Geosynthetics India*, 1–11. Austin, TX: International Geosynthetic Society.

ASTM. 2017a. *Standard practice for classification of soils for engineering purposes (unified soil classification system)*. ASTM D 2487. West Conshohocken, PA: ASTM.

ASTM. 2017b. *Standard test method for determining the shear strength of soil-geosynthetic and geosynthetic-geosynthetic interfaces by direct shear*. ASTM D 5321/D 5321M-21. West Conshohocken, PA: ASTM.

ASTM. 2021. *Standard test methods for laboratory compaction characteristics of soil using standard effort*. ASTM D 698. West Conshohocken, PA: ASTM.

Brennan, A. J., N. I. Thusyanthan, and S. P. G. Madabhushi. 2005. "Evaluation of shear modulus and damping in dynamic centrifuge tests." *J. Geotech. Geoenviron. Eng.* 131 (12): 1488–1497. https://doi.org/10.1061/(ASCE)1090-0241(2005)131:12(1488).

Carbone, L., J. P. Gourc, P. Carrubba, P. Pavanello, and N. Moraci. 2015. "Dry friction behaviour of a geosynthetic interface using inclined plane and shaking table tests." *Geotext. Geomembr.* 43 (4): 293–306. https://doi.org/10.1016/j.geotexmem.2015.05.002.

Chang, J. Y., and S. J. Feng. 2021. "Dynamic shear behaviors of textured geomembrane/nonwoven geotextile interface under cyclic loading." *Geotext. Geomembr.* 49 (2): 388–398. https://doi.org/10.1016/j.geotexmem.2020.10.010.

Chang, J. Y., and S. J. Feng. 2022. "A constitutive model for geosynthetic interfaces considering nonlinear softening behavior." *Comput. Geotech.* 143 (Mar): 104633. https://doi.org/10.1016/j.compgeo.2022.104633.

Chang, J. Y., S. J. Feng, Q. T. Zheng, and Y. Shen. 2021. "Cyclic shear behavior of GMB/GCL composite liner." *Geotext. Geomembr.* 49 (3): 593–603. https://doi.org/10.1016/j.geotexmem.2020.11.006.

Choudhury, D., and P. Savoikar. 2009. "Equivalent-linear seismic analyses of MSW landfills using DEEPSOIL." *Eng. Geol.* 107 (3–4): 98–108. https://doi.org/10.1016/j.enggeo.2009.05.004.

De, A., and T. F. Zimmie. 1998. "Estimation of dynamic interfacial properties of geosynthetics." *Geosynth. Int.* 5 (1–2): 17–39. https://doi.org/10.1680/gein.5.0112.

Dickinson, S., and R. W. I. Brachman. 2008. "Assessment of alternative protection layers for a geomembrane - geosynthetic clay liner (GM-GCL) composite liner." *Can. Geotech. J.* 45 (11): 1594–1610. https://doi.org/10.1139/T08-081.

Dos Santos, J. M., L. M. Amaral, and G. Martinho. 2023. "Effects of landfill age, climate, and size on leachate from urban waste landfills in Portugal: A statistics and machine learning analysis." *Waste Manage.* 172 (Dec): 192–207. https://doi.org/10.1016/j.wasman.2023.10.027.

Ewais, A. M. R., R. K. Rowe, S. Rimal, and H. P. Sangam. 2018. "17-year elevated temperature study of HDPE geomembrane longevity in air, water and leachate." *Geosynth. Int.* 25 (5): 525–544. https://doi.org/10.1680/jgein.18.00016.

Feng, S. J., J. Y. Chang, and H. X. Chen. 2018. "Seismic analysis of landfill considering the effect of GM-GCL interface within liner." *Soil Dyn. Earthquake Eng.* 107 (Mar): 152–163. https://doi.org/10.1016/j.soildyn.2018.01.025.

Feng, S. J., Y. Shen, Q. T. Zheng, and J. L. Shi. 2022. "Multi-functional direct shear apparatus for geosynthetic interfaces with its application on various GMB/GCL interfaces." *Acta Geotech.* 17 (3): 993–1008. https://doi.org/10.1007/s11440-021-01279-6.

Feng, S. J., J. L. Shi, Y. Shen, H. X. Chen, and J. Y. Chang. 2021. "Dynamic shear behavior of GMB/CCL interface under cyclic loading." *Geotext. Geomembr.* 49 (3): 657–668. https://doi.org/10.1016/j.geotexmem.2020.12.002.

Feng, S. J., and D. Z. Yang. 2012. "Seismic response of municipal waste landfills with bottom liner interface under different site conditions." [In Chinese.] *J. Tongji. Univ.* 40 (7): 1015–1019.

Fox, P. J., and J. D. Ross. 2011. "Relationship between NP GCL internal and HDPE GMX/NP GCL interface shear strengths." *J. Geotech. Geoenviron. Eng.* 137 (8): 743–753. https://doi.org/10.1061/(ASCE)GT.1943-5606.0000490.

Fox, P. J., J. D. Ross, J. M. Sura, and R. S. Thiel. 2011. "Geomembrane damage due to static and cyclic shearing over compacted gravelly sand." *Geosynth. Int.* 18 (5): 272–279. https://doi.org/10.1680/gein.2011.18.5.272.

Fox, P. J., S. S. Thielmann, A. Stern, and C. Athanassopoulos. 2014. "Interface shear damage to a HDPE geomembrane. I: Gravelly compacted clay liner." *J. Geotech. Geoenviron. Eng.* 140 (8): 04014039. https://doi.org/10.1061/(ASCE)GT.1943-5606.0001132.

Han, B. Y., J. M. Ling, X. Shu, W. M. Song, R. L. Boudreau, W. Hu, and B. Huang. 2019. "Quantifying the effects of geogrid reinforcement in unbound granular base." *Geotext. Geomembr.* 47 (3): 369–376. https://doi.org/10.1016/j.geotexmem.2019.01.009.

Hanson, J. L., T. S. Chrysovergis, N. Yesiller, and D. C. Manheim. 2015. "Temperature and moisture effects on GCL and textured geomembrane interface shear strength." *Geosynth. Int.* 22 (1): 110–124. https://doi.org/10.1680/gein.14.00035.

Hardin, B. O., and V. P. Drnevich. 1972. "Shear modulus and damping in soils: Design equations and curves." *J. Soil Mech. Found. Div.* 98 (7): 667–692. https://doi.org/10.1061/JSFEAQ.0001760.

Hsuan, Y. G., and R. M. Koerner. 1998. "Antioxidant depletion lifetime in high density polyethylene." *J. Geotech. Geoenviron. Eng.* 124 (6): 532–541. https://doi.org/10.1061/(ASCE)1090-0241(1998)124:6(532).

Ide, S., G. C. Beroza, D. R. Shelly, and T. Uchide. 2007. "A scaling law for slow earthquakes." *Nature* 447 (7140): 76–79. https://doi.org/10.1038/nature05780.

Kim, J., M. Riemer, and J. D. Bray. 2005. "Dynamic properties of geosynthetic interfaces." *Geotech. Test. J.* 28 (3): 288–296. https://doi.org/10.1520/GTJ11856.

Kyrikou, I., D. Briassoulis, M. Hiskakis, and E. Babou. 2011. "Analysis of photo-chemical degradation behaviour of polyethylene mulching film with pro-oxidants." *Polym. Degrad. Stab.* 96 (12): 2237–2252. https://doi.org/10.1016/j.polymdegradstab.2011.09.001.

Li, W. S., Y. Xu, Q. F. Huang, Y. Q. Liu, and J. C. Liu. 2021. "Antioxidant depletion patterns of high-density polyethylene geomembranes in landfills under different exposure conditions." *Waste Manage.* 121 (Jun): 365–372. https://doi.org/10.1016/j.wasman.2020.12.025.

Liang, F. Y., T. D. Li, Y. Qian, C. Wang, and Y. J. Jia. 2022. "Investigating the cushion effect of using pebble gravel in bridge foundations through laboratory cyclic direct shear tests." *J. Geotech. Geoenviron. Eng.* 148 (7): 04022051. https://doi.org/10.1061/(ASCE)GT.1943-5606.0002825.

Lin, H., L. L. Zhang, and Y. C. Xiong. 2018. "Research on shear strength of needle-punched GCL by simple-shear of composite liner." *Eng. Geol.* 244 (Oct): 86–95. https://doi.org/10.1016/j.enggeo.2018.07.022.

Liu, F. Y., H. Jiang, and J. Wang. 2021. "Experimental study on cyclic shear softening characteristics of gravel-geogrid interface." [In Chinese.] *Rock Soil Mech.* 42 (6): 1485–1492.

Liu, Z. L., J. Y. Shi, H. Lin, and Y. C. Zhang. 2023. "Strength characteristics of a smooth HDPE geomembrane/nonwoven geotextile interface based on a novel ring shear apparatus." *Polymers* 15 (11): 2497. https://doi.org/10.3390/polym15112497.

Martin, P. P., and H. B. Seed. 1982. "One-dimensional dynamic ground response analyses." *J. Geotech. Eng. Div.* 108 (7): 935–952. https://doi.org/10.1061/AJGEB6.0001316.

Mitchell, J. K., R. B. Seed, and H. B. Seed. 1990. "Kettleman Hills waste landfill slope failure. I: Liner-system properties." *J. Geotech. Eng.* 116 (4): 647–668. https://doi.org/10.1061/(ASCE)0733-9410(1990)116:4(647).

Nye, C. J., and P. J. Fox. 2007. "Dynamic shear behavior of a needle-punched geosynthetic clay liner." *J. Geotech. Geoenviron. Eng.* 133 (8): 973–983. https://doi.org/10.1061/(ASCE)1090-0241(2007)133:8(973).

Pavanello, P., P. Carrubba, and N. Moraci. 2018. "Dynamic friction and the seismic performance of geosynthetic interfaces." *Geotext. Geomembr.* 46 (6): 715–725. https://doi.org/10.1016/j.geotexmem.2018.06.005.

Pavanello, P., P. Carrubba, and N. Moraci. 2021. "The characterisation of geosynthetic interface friction by means of the inclined plane test." *Geotext. Geomembr.* 49 (1): 257–275. https://doi.org/10.1016/j.geotexmem.2020.10.027.

Pitanga, H. N., J. P. Gourc, and O. M. Vilar. 2009. "Interface shear strength of geosynthetics: Evaluation and analysis of inclined plane tests." *Geotext. Geomembr.* 27 (6): 435–446. https://doi.org/10.1016/j.geotexmem.2009.05.003.

Qian, X. D., and R. M. Koerner. 2010. "Modification to translational failure analysis of landfills incorporating seismicity." *J. Geotech. Geoenviron. Eng.* 136 (5): 718–727. https://doi.org/10.1061/(ASCE)GT.1943-5606.0000281.

Qian, X. D., J. Y. Shi, H. Liu, and Y. B. Zhu. 2011. "Failure interface behavior of multilayer landfill liner system." [In Chinese.] *Chin. J. Geotech. Eng.* 33 (6): 840–845.

Rowe, R. K. 2005. "Long-term performance of contaminant barrier systems." *Géotechnique* 55 (Jun): 631–678. https://doi.org/10.1680/geot.2005.55.9.631.

Rowe, R. K., M. Z. Islam, R. W. I. Brachman, D. N. Arnepalli, and A. R. Ewais. 2010. "Antioxidant depletion from a high density polyethylene geomembrane under simulated landfill conditions." *J. Geotech. Geoenviron. Eng.* 136 (7): 930–939. https://doi.org/10.1061/(ASCE)GT.1943-5606.0000302.

Rowe, R. K., M. Z. Islam, and Y. G. Hsuan. 2010. "Effects of thickness on the aging of HDPE geomembranes." *J. Geotech. Geoenviron. Eng.* 136 (2): 299–309. https://doi.org/10.1061/(ASCE)GT.1943-5606.0000207.

Rowe, R. K., and S. Rimal. 2008. "Depletion of antioxidants from a HDPE geomembrane in a composite liner." *J. Geotech. Geoenviron. Eng.* 134 (1): 68–78. https://doi.org/10.1061/(ASCE)1090-0241(2008)134:1(68).

Rowe, R. K., H. P. Sangam, and C. B. Lake. 2003. "Evaluation of an HDPE geomembrane after 14 years as a leachate lagoon liner." *Can. Geotech. J.* 40 (3): 536–550. https://doi.org/10.1139/t03-019.

Rowe, R. K., and M. Shoaib. 2018. "Durability of HDPE geomembrane seams immersed in brine for three years." *J. Geotech. Geoenviron.*

Eng. 144 (2): 04017114. https://doi.org/10.1061/(ASCE)GT.1943-5606.0001817.

Sarkar, G., and A. Sadrekarimi. 2022. "Cyclic shearing behavior and dynamic characteristics of a fibrous peat." *Can. Geotech. J.* 59 (5): 688–701. https://doi.org/10.1139/cgj-2020-0516.

Sirieix, C., F. Genelle, C. Barral, N. Touze-Foltz, J. Riss, and B. Begassat. 2016. "Characterizing the aging of a geosynthetic clay liner through electrical resistivity." *Can. Geotech. J.* 53 (3): 423–430. https://doi.org/10.1139/cgj-2015-0111.

Stark, T. D., and A. R. Poeppel. 1994. "Landfill liner interface strengths from torsional-ring-shear tests." *J. Geotech. Eng.* 120 (3): 597–615. https://doi.org/10.1061/(ASCE)0733-9410(1994)120:3(597).

Suits, L. D., and Y. G. Hsuan. 2003. "Assessing the photo-degradation of geosynthetics by outdoor exposure and laboratory weatherometer." *Geotext. Geomembr.* 21 (2): 111–122. https://doi.org/10.1016/S0266-1144(02)00068-7.

Take, W. A., R. K. Rowe, R. W. I. Brachman, and D. N. Arnepalli. 2015. "Thermal exposure conditions for a composite liner with a black geomembrane exposed to solar radiation." *Geosynth. Int.* 22 (1): 93–109. https://doi.org/10.1680/gein.14.00034.

Tian, K., C. H. Benson, J. M. Tinjum, and T. B. Edil. 2017. "Antioxidant depletion and service life prediction for HDPE geomembranes exposed to low-level radioactive waste leachate." *J. Geotech. Geoenviron. Eng.* 143 (6): 04017011. https://doi.org/10.1061/(ASCE)GT.1943-5606.0001643.

Uenishi, K. 2018. "Physics of earthquake disaster: From crustal rupture to building collapse." *Annu. Rev. Earth Planet. Sci.* 46 (1): 387–408. https://doi.org/10.1146/annurev-earth-082517-010217.

Vieira, C. S., M. L. Lopes, and L. M. Caldeira. 2013. "Sand-geotextile interface characterisation through monotonic and cyclic direct shear tests." *Geosynth. Int.* 20 (1): 26–38. https://doi.org/10.1680/gein.12.00037.

Wang, J., F. Y. Liu, P. Wang, and Y. Q. Cai. 2016. "Particle size effects on coarse soil-geogrid interface response in cyclic and post-cyclic direct shear tests." *Geotext. Geomembr.* 44 (6): 854–861. https://doi.org/10.1016/j.geotexmem.2016.06.011.

Wang, J., F. Y. Liu, Q. T. Zheng, Y. Q. Cai, and C. F. Gou. 2021. "Effect of aperture ratio on the cyclic shear behaviour of aggregate-geogrid interfaces." *Geosynth. Int.* 28 (2): 158. https://doi.org/10.1680/jgein.20.00038.

Xue, Q., Q. Zhang, Z. Z. Li, and K. Xiao. 2013. "The tension and puncture properties of HDPE geomembrane under the corrosion of leachate." *Materials* 6 (9): 4109–4121. https://doi.org/10.3390/ma6094109.

Yegian, M. K., and A. M. Lahlaf. 1992. "Dynamic interface shear strength properties of geomembranes and geotextiles." *J. Geotech. Eng.* 118 (5): 760–779. https://doi.org/10.1061/(ASCE)0733-9410(1992)118:5(760).